Korean J. Chem. Eng., 39(9), 2368-2378 (2022)
DOI: 10.1007/s11814-022-1136-x

pISSN: 0256-1115
eISSN: 1975-7220

H_2S adsorption performance of alkali lignocarbon/PVA composite membrane

Youjing Li*, Fen Li*,,†, Menglong Zheng*, Hong Yan*,†, and Qianliang Liu***

*School of Materials Science and Chemical Engineering, Harbin University of Science and Technology, Harbin, 150040
**Guangdong Province Engineering Laboratory for Air Pollution Control, Guangzhou, 510655
(*Received 28 October 2021 • Revised 23 February 2022 • Accepted 2 April 2022*)

Abstract−In this work, lignin carbon-based membranes were prepared for H_2S adsorption. Alkali lignin was carbonized to obtain alkali lignocarbon (CLA). Using the CLA and polyvinyl alcohol (PVA) as raw materials, glycerol and water as plasticizers, and nano-CuO and Cu^{2+} as dopants, CLA/PVA, CuO-CLA/PVA-1, and Cu-CLA/PVA-2 composite membranes were prepared by solution casting method. The structures of these membranes and their H_2S adsorption properties were then analyzed. The results show that with a membrane solution water-alcohol ratio of 3 : 1 and 2 wt% CLA content, the prepared CLA/PVA membrane can adsorb H_2S for 30 min. The CuO-CLA/PVA-1 and Cu-CLA/PVA-2 membranes, which were obtained after doping with nano-CuO and Cu^{2+}, demonstrate significantly improved deodorization performance compared with that of CLA/PVA. The Cu-CLA/PVA-2 membrane can adsorb H_2S for up to 75 min and also demonstrates better mechanical properties. The H_2S adsorption capacity of this membrane is up to 0.27 mol/kg. Structural analysis shows that the veneers of the three composite membranes are smooth and that doped copper is evenly distributed in the membranes as nano-CuO. The surface functional groups of the CLA/PVA, CuO-CLA/PVA-1, and Cu-CLA/PVA-2 membranes are similar and play a positive role in H_2S adsorption. Nano-CuO is the main active site for H_2S adsorption in the Cu-containing composite membranes.

Keywords: Alkali Lignocarbon, Polyvinyl Alcohol, Composite Membrane, H_2S Adsorption

INTRODUCTION

Many malodorous gases are emitted during industrial production and in daily life, which negatively impacts the environment and human health. Adsorption methods are widely used for odor pollution treatment due to their simple and reliable operation. Among these methods, activated carbon is the most commonly used odor adsorption material [1,2]. Activated carbon is mostly used in granular or powder form for industrial production and scientific research. However, in recent years, carbon membranes have attracted an increasing amount of attention due to their abundant pores and adjustable pore size. Carbon membranes have good separation performance for small molecular gases with similar molecular scales and can be used in processes such as hydrogen recovery, air separation, alkane/olefin separation, and acid gas adsorption from natural gas [3,4]. Two different processes can occur in the adsorption and separation of gases by carbon membranes: one process is the adsorption of gas on the carbon membrane, which leads to surface diffusion and gas separation. The other process is the integration of membrane adsorption and membrane separation processes in a so-called adsorption separation membrane. Adsorption separation membranes are expected to improve membrane separation performance. Carbon membrane adsorption has the advantages of specific selectivity and easy scalability. This membrane technology is therefore conducive to industrial production and use [5]. However, existing carbon membrane research mainly focuses on the separation of gas, and there is less research in the field of waste gas adsorption.

There are two main types of carbon membranes: homogeneous carbon membranes and composite carbon membranes. Conventional preparation methods involve directly coating a liquid polymer membrane solution on the surface of a support to form a carbon membrane, which is prepared through pretreatment, drying, carbonization, and post-treatment processes [6]. For example, Sim et al. [7] used hyperbranched polyimide (PI) as a carbon membrane precursor to investigate the effect of branching on the pore size distribution and gas separation performance of their carbon membrane. Their results showed that increasing the PI branching degree enhanced the rigidity of the molecular chains in the membrane. This lowered the carbon membrane density, which was conducive to forming micropores, improving gas diffusion selectivity, and enhancing the CO_2/CH_4 separation coefficient to as high as 52. To simplify the preparation process, Somsesta et al. [8] combined activated carbon with a cellulose solution dissolved in lithium chloride/N,N-dimethylacetamide to prepare an activated carbon/cellulose (ACC) composite biosorption membrane by solution casting. Methylene blue was used as a model pollutant to detect the adsorption behavior of this biocomposite membrane, and its maximum methylene blue adsorption capacity reached 103.66 mg g^{-1}.

However, it has been reported that most of the carbon sources used in carbon membranes are petrochemical products and that prepared carbon membrane materials have poor environmental absorbability and high raw material costs. To address this issue, Liu et al. [9] prepared biomass-based carbon membranes under controlled thermal decomposition conditions using two-layer cowhide as the carbon source. Their carbon membranes had an optimal lead ion removal rate of up to 99.9% and an adsorption capacity of

†To whom correspondence should be addressed.
E-mail: hgxylf@126.com, yanhong204821@aliyun.com

32.76 mg g^{-1}. However, the carbon source of this research was layered cowhide, and raw materials in nature that have similar layered structures are limited. Therefore, the prospect of industrial scale-up using this membrane material is not optimistic.

The use of biomass resources with rich reserves as carbon sources shows great promise. As a raw material, corn straw has a wide range of sources and its fiber structure contains many functional groups that are mostly selectively retained after charring. These include hydroxyl, carboxyl, and amine groups, which can be used as active adsorption sites [10]. As a natural and abundant biological macromolecule, lignin is available from a wide range of sources. Because of its high carbon content and benzene ring skeleton, lignin is an ideal precursor for carbon-based functional materials [11,12]. Lignin sulfonates contain a large number of metal ions, and these metal ions can be used as activators to obtain pores during the charring process. Lignin charcoal has a high porosity and is mainly microporous. Because of its relatively small molecular weight, the microscopic morphology of alkali lignin is easily regulated, so lignin porous carbons with unique morphologies can be prepared [13]. Some researchers have reported using lignin in the preparation of carbon membranes. For example, Zhang et al. [14] and Zhong [15] used different lignin ratios with formaldehyde and phenol to synthesize phenolic resins for the fabrication of charred membranes. Chau et al. [16] slowly combined a graphene oxide solution and a lignin solution. After casting the mixed solution into the membrane, it was carbonized and activated under a nitrogen atmosphere to form a carbon membrane. These lignin carbon membranes have high specific surface areas and ideal capacitance behavior. However, lignin carbon membrane research has mainly focused on the field of electrochemistry, and little research has been reported for gas adsorption membranes [17].

In this work, alkali lignin was used as a carbon source to prepare an alkali lignocarbon (CLA) membrane for the adsorption of the malodorous gas H_2S. The membrane process conditions were optimized and the structure of the composite membrane was analyzed. To prepare the membrane, CLA was compounded with a high molecular weight polymer and active materials to enhance its deodorizing functionality and act as a carrier for the deodorizing functional materials. Furthermore, the mechanical properties of the membrane were tested. The results provided herein offer an application pathway for the functionalized utilization of alkali lignin.

MATERIALS AND METHODS

1. Materials and Reagents

Alkali lignin and sodium lignosulfonate were purchased from Macklin (China), and corn stalks were obtained from rural areas around Harbin, China. The alkali lignin, sodium lignosulfonate, and corn straw were charred in a tube furnace under a N_2 atmosphere at 400 °C for 3 h, using a heating rate of 5 °C/min to obtain carbon (C) products. The resulting alkaline lignin char was denoted CLA, the sodium lignosulfonate char was denoted CSL, and the straw char was denoted SC. Polyvinyl alcohol (PVA) (1788 low viscosity, alcoholysis degree 87.0-89.0 mol mol^{-1}) was purchased from Macklin (China). PVA was heated in a water bath at 90 °C for 4 h to obtain a 5 wt% PVA aqueous solution. Nano copper oxide (nano-CuO, 99.5%, 40 nm, spherical) was purchased from Macklin (China), copper nitrate ($Cu(NO_3)_2{\cdot}3H_2O$) was purchased from Tianjin Basmai Chemical Co., Ltd., and analytically pure glycerol was purchased from Xilong Chemical Co., Ltd.

2. Preparation of Composite Membranes

The composite membrane preparation process is shown in Fig. 1.

(1) Distilled water and 5 wt% PVA solution were added to a beaker at a volume ratio (mL : mL) of 1 : 1, 1.5 : 1, 2 : 1, 2.5 : 1, or 3 : 1. Each solution was mixed and stirred with a magnetic stirrer for 30 min. (2) 0.25-2 wt% CLA (wt% based on the amount of solu-

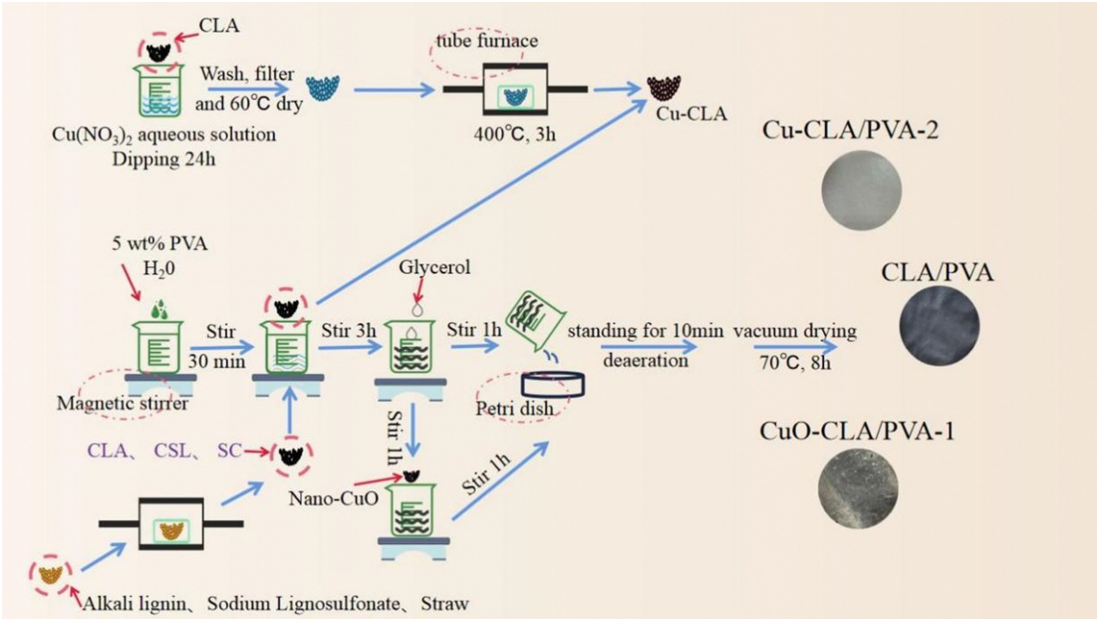

Fig. 1. Schematic diagram of the composite membrane preparation process.

tion) was added to the mixture, which was stirred for an additional 3 h. (3) 0.1 mL propanetriol was added to the solution as a plasticizer and stirred for 1 h. (4) After stirring, the mixture was poured onto a 9×9 cm Petri dish, allowed to defoam for 15 min, and placed in a 70 °C vacuum drying oven for 8 h. After drying, the membrane was cooled, peeled out of the Petri dish, and stored in a sealed bag. This membrane was denoted CLA/PVA. CSL/PVA and SC/PVA membranes were prepared using the same process.

To prepare CuO-doped membranes, the same procedure was followed with one additional step: after step (3), 5-30 wt% nano-CuO (wt% based on the amount of CLA) was added to the solution, which was then stirred for 1 h. This membrane was denoted CuO-CLA/PVA-1.

To prepare Cu^{2+}-doped membranes, a certain amount of CLA was added to an aqueous copper nitrate solution, using concentrations necessary to obtain 5-30 wt% copper-impregnated CLA. The CLA was impregnated for 24 h, washed and filtered to remove surface impurities, dried at 60 °C, and then roasted at 400 °C for 3 h in a tube furnace under N_2 protection to obtain Cu-CLA. The membranes were prepared using the same process as that used for the CLA/PVA membranes, with Cu-CLA replacing CLA in preparation step (2). This prepared material was denoted Cu-CLA/PVA-2.

3. H_2S Adsorption Performance Tests

The composite membrane H_2S adsorption experimental system is shown in Fig. 2. H_2S (1,000±5 ppm) standard gas produced by Dalian Dart Gas Co., Ltd. was used for testing. In a typical test, a composite membrane was cut into 3 cm diameter circular test samples, which were installed in a Plexiglas reactor. The H_2S flow rate was fixed at 8 mL min^{-1} by adjusting the gas cylinder valve. After flow rate stabilization, H_2S was passed into the plexiglass reactor, and data recording was initiated. Samples were removed at certain intervals from the outlet of the plexiglass reactor, and the concentration of H_2S at the outlet was detected using gas chromatography (GC-9160, Shanghai Ouhua Analytical Instrument Factory). The inlet gas flow was stopped when the outlet H_2S concentration reached 20.0 ppm, and the performance of each membrane material in H_2S removal was assessed based on the time from the start of adsorption to the stop of adsorption. The penetration adsorption amount of H_2S was calculated using Eq. (1).

$$\mathrm{Cap(PT)} = \frac{\mathrm{PT} \times \mathrm{FR} \times C_{H_2S}}{34 \times \mathrm{W} \times 10^{-3}} \quad (1)$$

where Cap(PT) is the H_2S penetration adsorption amount, mol/kg; PT is the penetration time, min; FR is the gas flow rate, mL/min; C_{H_2S} is H_2S gas concentration, 1.518 mg/L (1,000 ppm); W is the mass of the membrane, g.

4. Testing and Characterization

Scanning electron microscopy (SEM) and energy-dispersive X-ray spectroscopy (EDS) analyses were performed using a JSM-6380LV scanning electron microscope (JEOL, Japan) and an auxiliary projection electron spectrometer (Oxford Instruments, UK). SEM samples were subjected to vacuum filtration and coated with gold before analysis. EDS was used to investigate the elements on the sample surfaces after H_2S adsorption.

X-ray diffraction (XRD) analysis was carried out using a D8 Advance X-ray diffractometer (BRUKER, Germany) with a Cu target, a Kα radiation source, a tube voltage of 40 kV, a tube current of 40 mA, a 2θ scanning range of 5-75°, and a scanning speed of 2° min^{-1}. XRD was used to analyze the crystallographic characteristics and physical phase composition of the membrane materials.

The surface functional groups of the composite membranes were analyzed by Fourier-transform infrared spectroscopy (FT-IR) using a T60SXBFTIR (Nicolet, USA). In each test, 1-2 mg sample was used, and each sample was compressed to 0.8-1 GPa (8-10 T cm^{-2}) for 2-5 min.

The mechanical properties of the membranes were tested using an INSTRON-1121 material testing machine. Membrane samples with a length of 60 mm were tested using a stretching rate of 10 mm min^{-1}. After each test, the thickness and width of the membrane samples were measured in three places to obtain average values. For each membrane, the elongation at break and tensile strength were tested 5 times to obtain average values.

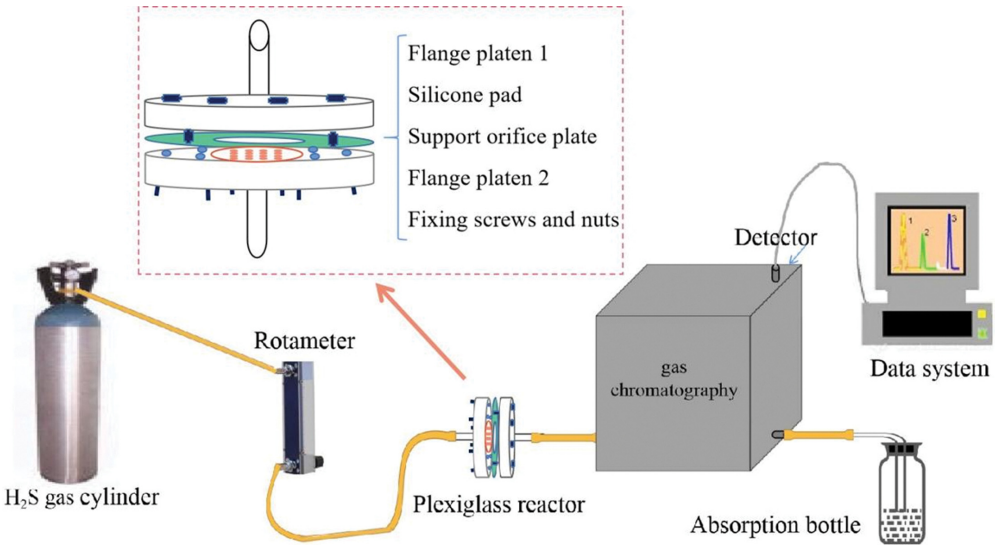

Fig. 2. Schematic diagram of H_2S adsorption experiments.

RESULTS AND DISCUSSION

1. H_2S Adsorption Performance of Composite Membranes

1-1. Effect of Different Charcoal-based Composite Membranes on H_2S Adsorption Performance

Lignin is a natural biomolecule with abundant reserves, high carbon content, and a benzene ring backbone. Thus, lignin is an ideal precursor for the preparation of carbon-based functional materials [13]. Lignin sulfonate contains a large amount of sodium, calcium, ammonium, and other metal ions, and these metal ions can be used as activators to create pores during the charcoal-making process [18]; Due to its relatively low molecular weight, the use of alkaline lignin leads to the generation of relatively small carbon particles with more surface active sites, making it ideal for adsorption reactions [13]. Corn stover is a widely available material, and its fiber structure contains many functional groups. Most of these functional groups, including hydroxyl, carboxyl, and amine groups, can be selectively retained after charring. These functional groups can then be used as adsorption active sites [19]. To study the deodorization performance of different carbon membranes, CLA/PVA, CSL/PVA, and SC/PVA composite membranes were prepared by using alkali lignin carbon, sulfonate lignin carbon, and straw carbon as raw materials. The effects of these different materials in membranes prepared using differing PVA to H_2O ratios on H_2S adsorption performance were compared, as shown in Fig. 3.

As shown in Fig. 3, all three membranes have a significant adsorption effect on H_2S, with adsorption times of about 10 min. Compared with CSL/PVA and SC/PVA, CLA/PVA has better H_2S adsorption performance, demonstrating the longest H_2S adsorption time of up to 15 min. Alkali lignin contains up to 60% carbon and has a molecular structure similar to that of bituminous coal. Moreover, alkali lignin is weakly alkaline when dissolved in water. The alkali lignin carbon prepared by carbonization has a large specific surface area and small particle size. This CLA also has oxygen-containing active functional groups on its surface, and

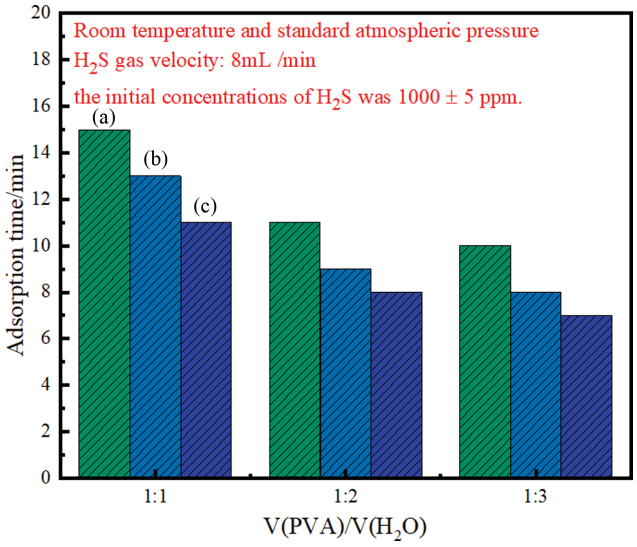

Fig. 3. H_2S adsorption performance of CLA/PVA, CSL/PVA, and SC/PVA membranes ((a) CLA/PVA; (b) CSL/PVA; (c) SC/PVA).

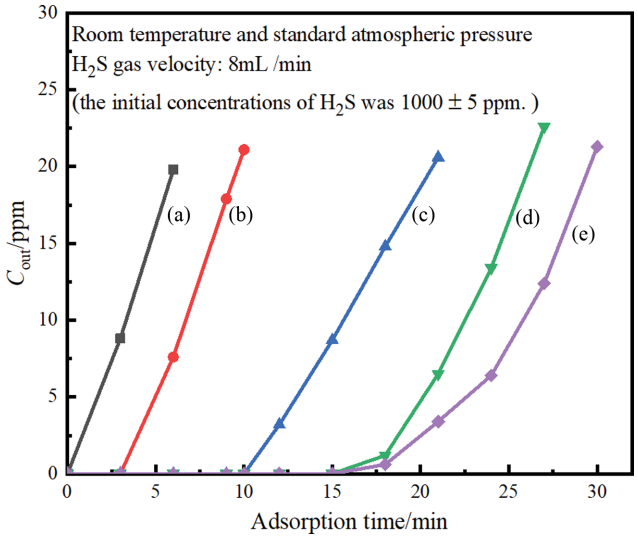

Fig. 4. H_2S adsorption time curves of CLA/PVA membranes with different CLA content ((a) 0.25%; (b) 0.5%; (c) 1.0%; (d) 1.5%; (e) 2.0%).

the existence of these oxygen-containing functional groups facilitates the adsorption of H_2S [20]. In addition, less alkali lignin is currently available for effective use, and this lignin is usually disposed of as fuel. Therefore, based on the deodorization performance testing reported in Fig. 3 and the need to improve alkali lignin utilization, alkali lignin carbon was selected to prepare composite membranes for further experimental study.

1-2. Effect of CLA Content on CLA/PVA Membrane H_2S Adsorption Performance

Fig. 4 shows the effect of CLA content on the performance of CLA/PVA membranes for H_2S adsorption. These CLA/PVA membranes demonstrate the ability to adsorb H_2S for longer periods of time with increasing CLA content. The CLA/PVA membrane with 2 wt% CLA adsorbs H_2S for up to 30 min. Increasing the membrane CLA content means that more CLA particles are dispersed on the mesh structure of the substrate, which is composed of PVA, water, and glycerol bonded by hydrogen bonds. A large number of nanoscale boundary surface pores are formed between the uniformly dispersed CLA particles and the mesh structure substrate due to microphase separation. Together with the regular pore channels of CLA, these pores modify and shorten the diffusion path of gas molecules in the carbon membrane. This significantly improves gas permeation flux, increases the number of active adsorption sites, and improves the overall adsorption effect. When the CLA content was further increased above 2 wt%, CLA residues were found on the surface of the Petri dish after removing the membrane and the black CLA powder adhered to the glass reactor during adsorption experiments. Therefore, 2 wt% CLA is the optimal CLA concentration for achieving the best H_2S adsorption performance.

Fig. 5 shows the effect of CLA content on the mechanical properties of the CLA/PVA membranes. The tensile strength and elongation at break values of CLA/PVA show decreasing trends with increasing CLA content. This is because CLA is a rigid particle. Thus, increasing the CLA content in PVA leads to the presence of

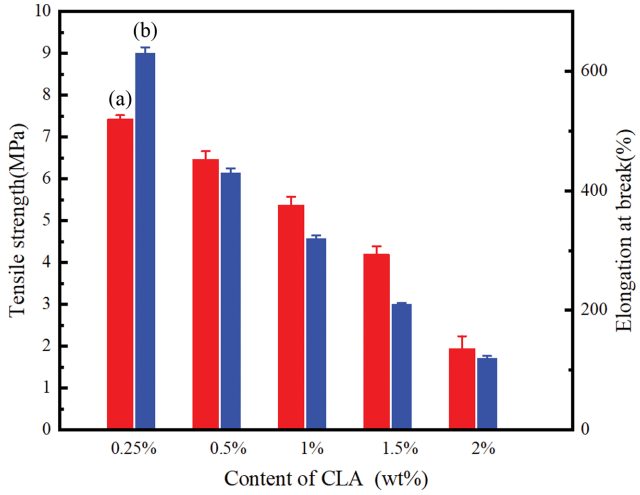

Fig. 5. Effect of CLA content on the mechanical properties of CLA/PVA (VH_2O/V(PVA)=3 : 1) ((a) tensile strength; (b) elongation at break).

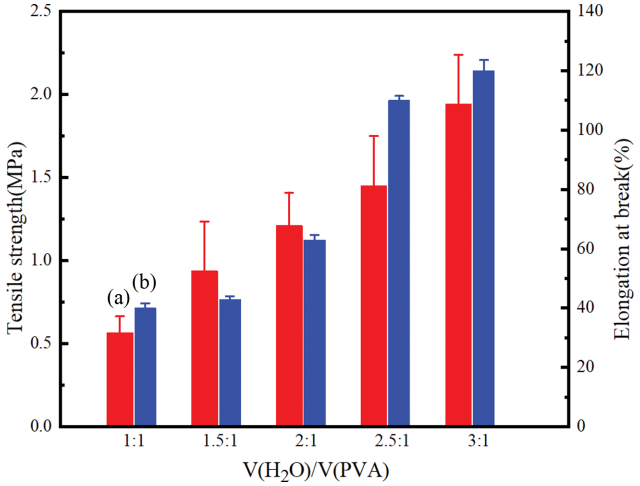

Fig. 7. Effect of the water-alcohol ratio on the mechanical properties of CLA/PVA membranes with 2 wt% CLA content ((a) tensile strength; (b) elongation at break).

more defective points in the membrane, resulting in lower mechanical strength and elongation at break. The tensile strength of the CLA/PVA membrane with 2 wt% CLA is 1.94 MPa and its elongation at break is 120%. These values are close to the reported data for lignin-alginate based films and PVA/lignin blended films [21,22], indicating that this prepared lignin carbon membrane is promising for engineering applications.

1-3. Effect of Membrane Solution Water-to-alcohol Ratio on CLA/PVA H_2S Adsorption Performance

Plasticizers can form hydrogen bonds with the hydroxyl groups of PVA. This destroys the hydrogen bonds within PVA and reduces its melting point. Glycerol is the most commonly used plasticizer for PVA, but its plasticizing effect is not satisfactory by itself. However, by combining glycerol with other plasticizers, a synergistic plasticizing effect can be obtained [23]. In this paper, water and glycerol compounding was used to improve the properties of the prepared composite membranes. Changing membrane properties impacts their structure and performance, so the effect of the water-to-alcohol ratio (V(H_2O)/V(PVA)) of the membrane precursor solution on the CLA/PVA H_2S adsorption performance was investigated, as shown in Fig. 6. Increasing the V(H_2O)/V(PVA) ratio improves the CLA/PVA H_2S adsorption time. When a 3 : 1 V(H_2O)/V(PVA) ratio is used, the H_2S adsorption time of CLA/PVA reaches 30 min. The PVA-based CLA/PVA membrane contains a large number of hydrophilic groups. H_2O plasticizes PVA polymer chains by reducing the intramolecular and intermolecular hydrogen bonding of PVA via the formation of hydroxyl groups. This reduces the crystallinity of PVA and increases the free volume of the membrane, which is more conducive to the uniform distribution of CLA in the reticular hydrogen-bonded structure composed of PVA, water, and propanetriol [24,25]. Thus, the adsorption performance of CLA is enhanced by increasing the V(H_2O)/V(PVA) ratio.

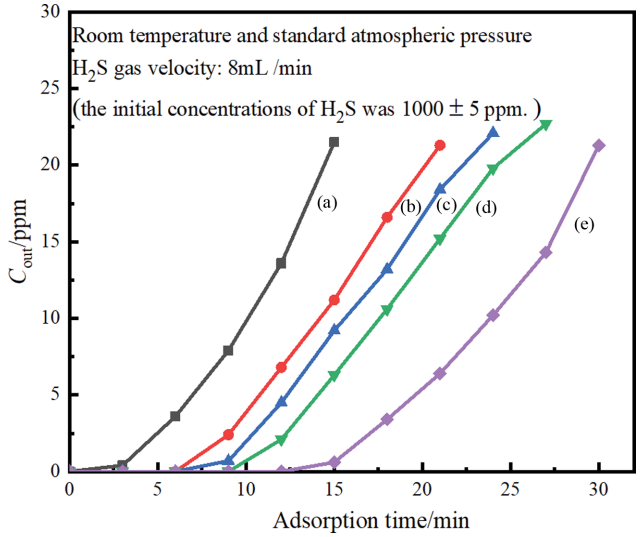

Fig. 6. H_2S adsorption time curve of CLA/PVA membranes prepared using precursor solutions with different water-alcohol ratios and 2 wt% CLA ((a) V(H_2O)/V(PVA)=1 : 1; (b) V(H_2O)/V(PVA)=1.5 : 1; (c) V(H_2O)/V(PVA)=2 : 1; (d) V(H_2O)/V(PVA)=2.5 : 1; (e) V(H_2O)/V(PVA)=3.0 : 1).

Fig. 7 shows the effect of the water-to-alcohol ratio on the mechanical properties of the CLA/PVA membranes. The tensile strength of CLA/PVA increases from 0.56 MPa to 1.94 MPa and the elongation at break increases from 43% to 120% as V(H_2O)/V(PVA) increases from 1 : 1 to 3 : 1. This is because the insertion of H_2O molecules into the PVA breaks the hydrogen bonds between PVA molecules, which weakens the interaction force between PVA molecules and improves the flexibility of the PVA molecular chains [26,27].

1-4. Effect of Copper Doping on H_2S Adsorption Performance of CLA/PVA

1-4-1. H_2S Adsorption Performance of CuO-CLA/PVA-1

To further improve the adsorption performance of the CLA/PVA membranes, nano-CuO (which is known to strongly adsorb H_2S) was co-blended into the membrane precursor solution to obtain CuO-CLA/PVA-1 membranes. The effect of nano-CuO content on H_2S adsorption by the CuO-CLA/PVA-1 membranes was

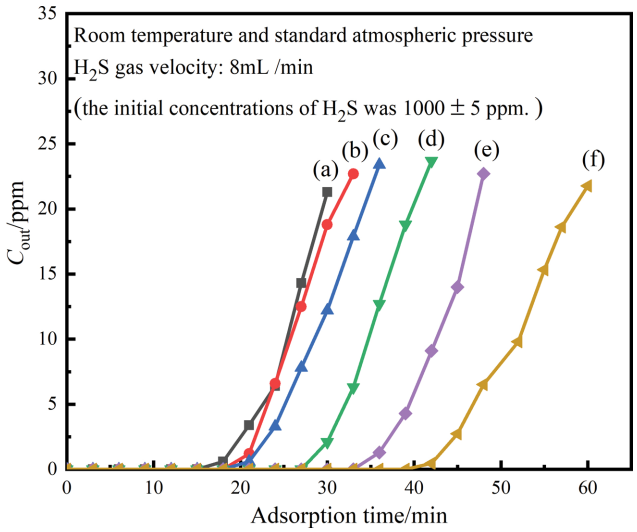

Fig. 8. H_2S adsorption time curves of CuO-CLA/PVA-1 membranes with varying nano-CuO content ((a) No CuO content; (b) CuO : CLA=5%; (c) CuO : CLA=10%; (d) CuO : CLA=15%; (e) CuO : CLA=20%; (f) CuO : CLA=30%).

investigated. As shown in Fig. 8, the adsorption of H_2S by CuO-CLA/PVA-1 is better than that of CLA/PVA. Furthermore, the maximum H_2S adsorption time by CuO-CLA/PVA-1 gradually increases with increasing nano-CuO content. The CuO-CLA/PVA-1 H_2S adsorption time of H_2S reaches 60 min with 30 wt% nano-CuO. These results demonstrate that CuO is an important active component of CuO-CLA/PVA-1. H_2S is a weakly acidic gas, so when H_2S molecules flow through the pores and surface of CuO-CLA/PVA-1, the alkaline copper oxide captures the H_2S molecules. The room-temperature reactions between H_2S and CuO lead to the formation of copper-containing sulfides such as CuS and Cu_2S, resulting in the removal of H_2S [28]. Furthermore, the unique surface interface, small size, and quantum tunneling effect of nano-CuO affect the force between the PVA polymer chains and thus change the internal structure of the composite membrane at the molecular level. This is beneficial for enhancing the adsorption of H_2S by the composite membrane [29-33].

Fig. 9 shows the effect of CuO content on the mechanical properties of the CuO-CLA/PVA-1 membranes. The tensile strength and elongation at break values of the CuO-CLA/PVA-1 membranes are higher than those of CLA/PVA. As the CuO content in the membranes increases from 5 wt% to 30 wt%, their tensile strength decreases from 4.35 MPa to 3.12 MPa, while their elongation at break increases from 390% to 440% and then decreases to 240%. The higher tensile strength and elongation at break values are due to the small size of the CuO nanoparticles, their high specific surface area, and the large number of oxygen-containing functional groups on their surface. These functional groups have a strong bonding or coupling effect with the hydroxyl groups of PVA, which improves the strength of the CuO-CLA/PVA-1 membranes [34]. The elongation at break initially increases and then decreases. This transient enhancement is due to the increasing CuO content weakening the original phase separation structure. However, if the CuO content of the membrane is too high, a phase separation phenomenon reemerges. This phenomenon negatively affects the elongation at break of the membrane.

1-4-2. H_2S Adsorption Performance of Cu-CLA/PVA-2

In the previous section, a co-blending method was used to dope nano-CuO into the CLA/PVA membranes. Here, an equal volume immersion method was used to load copper onto CLA. During membrane fabrication, the adsorbed $Cu(NO_3)_2$ decomposed into the active component CuO. The H_2S adsorption performance of the resulting Cu-CLA/PVA-2 composite membranes was then investigated. Fig. 10 shows the effect of Cu loading on the H_2S adsorption performance of the Cu-CLA/PVA-2 membranes. The addition of Cu-CLA enhances the H_2S adsorption performance of Cu-CLA/PVA-2 compared to that of CLA/PVA. With increasing Cu loading, the H_2S adsorption time of the Cu-CLA/PVA-2 membrane first increases and then decreases, reaching a maximum H_2S

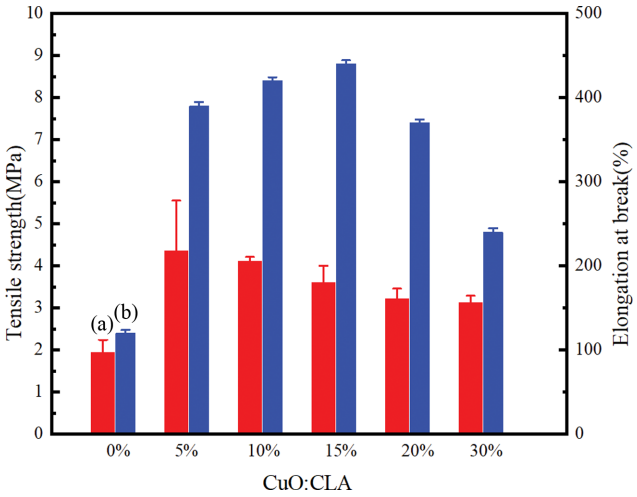

Fig. 9. Mechanical properties of CuO-CLA/PVA-1 membranes with varying nano-CuO content ((a) tensile strength; (b) elongation at break).

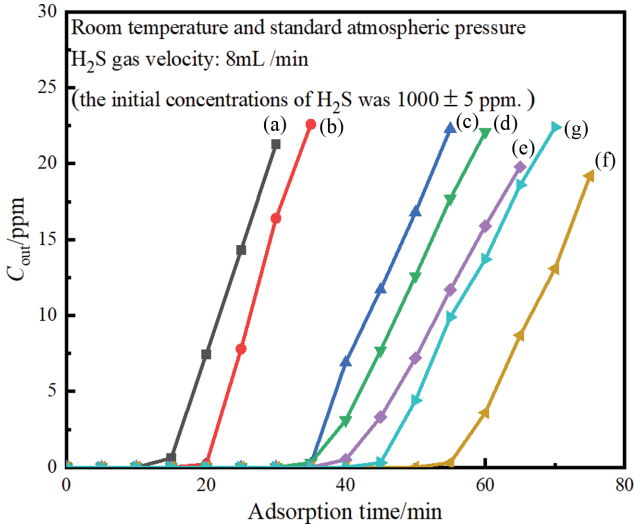

Fig. 10. H_2S adsorption time curves of Cu-CLA/PVA-2 membranes with different Cu loadings ((a) No CuO content; (b) 5%; (c) 10%; (d) 15%; (e) 20%; (f) 25%; (g) 30%).

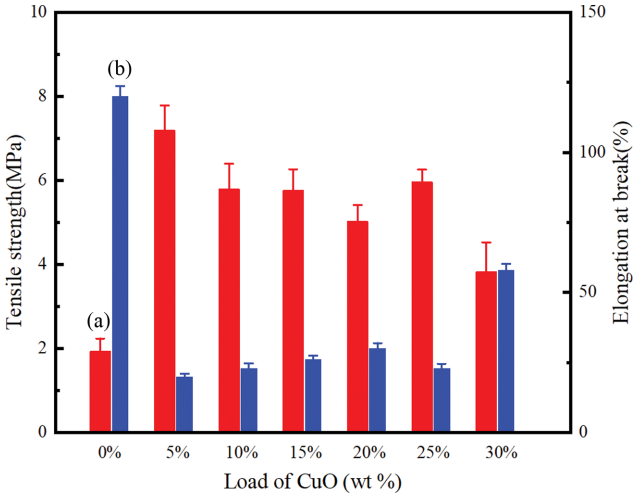

Fig. 11. Mechanical properties of Cu-CLA/PVA-2 membranes with different Cu loadings ((a) tensile strength; (b) elongation at break).

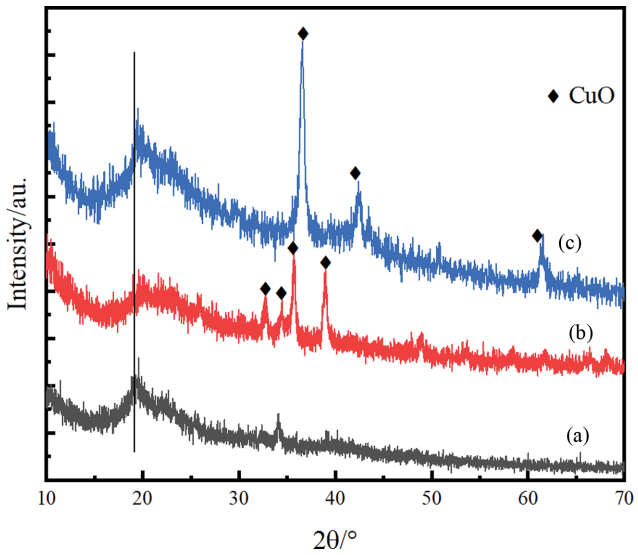

Fig. 12. X-ray diffraction (XRD) patterns of prepared membranes ((a) CLA/PVA; (b) CuO-CLA/PVA-1; (c) Cu-CLA/PVA-2).

adsorption time of 75 min with 25 wt% Cu on CLA. Moreover, the H_2S adsorption capacity of Cu-CLA/PVA-2 reaches 0.27 mol/kg. Based on these results, the long-term malodor gas treatment research results of our group, and some other related literature, this Cu-CLA/PVA-2 membrane exhibits ideal adsorption performance [35-37]. With 30 wt% Cu, the adsorption effect of Cu-CLA/PVA-2 decreases. This is because the CuO particles formed after high-temperature roasting can separate from the CLA and agglomerate, which blocks some of the CLA pore channels and increases membrane permeation resistance. This reduces the uniformity of the Cu-CLA particles on the surface and inside the membrane, leading to a decline in H_2S adsorption.

Fig. 11 shows the effect of Cu loading on the mechanical properties of the Cu-CLA/PVA-2 membranes. The tensile strength values of the Cu-CLA/PVA-2 membranes are higher than that of CLA/PVA, while their elongation at break values are generally lower than that of CLA/PVA. Increasing the Cu loading from 5 wt% to 30 wt% decreases the tensile strength of Cu-CLA/PVA-2 from 7.19 MPa to 3.83 MPa and increases the elongation at break from 20% to 58%, showing an inverse trend. The good mechanical properties of Cu-CLA/PVA-2 may be due to the changes in polymer structure and morphology caused by Cu-CLA. These changes are due to the improved polymer molecular interactions and interfacial interactions between Cu-CLA and the -OH groups of PVA. The loaded Cu is mainly distributed on the surface of CLA, which increases the CLA particle size. These large particles are embedded in the hydrogen-bonded mesh structure of PVA, water, and propanetriol, which reduces the elongation at break.

2. Structural Analysis

2-1. XRD Analysis

XRD characterization was performed to investigate the crystal structures of the CLA/PVA, CuO-CLA/PVA-1, and Cu-CLA/PVA-2 composite membranes, as shown in Fig. 12. All three composite membrane samples show diffraction peaks at a 2θ value of 19.5°, corresponding to the (101) crystal plane of PVA. The full widths at half maximum (FWHM) and low intensities of these peaks indicate the semi-crystalline nature of the PVA [38]. No diffraction peaks are attributed to the lignin carbon component in the composite membranes, indicating a low degree of order. Unlike CLA/PVA, the CuO-CLA/PVA-1 membrane shows distinct diffraction peaks at 2θ values of 35.7° and 38.9°, which are attributed to the CuO (002) and (111) crystal planes, respectively (PDF card no. 05-0667). Weaker diffraction peaks at 32.74° and 34.43° further confirm the presence of CuO. For Cu-CLA/PVA-2, strong diffraction peaks appear at 2θ values of 36.42°, 42.30°, and 61.34°, and these peaks are attributed to the CuO (111), (200), and (220) crystal planes, respectively (PDF card no. 05-0677). These results demonstrate the presence of CuO in both CuO-CLA/PVA-1 and Cu-CLA/PVA-2. The crystal growth of copper oxide in the two membranes differs due to the different doping methods. The FWHM of the CuO (111) diffraction peak and the Scherrer equation were used to determine that the surface CuO grain size of Cu-CLA/PVA-2 is 13.6 nm. The FWHM of the CuO (002) diffraction peak and the Scherrer equation were used to determine that the CuO-CLA/PVA-1 surface CuO grain size is 16.2 nm.

2-2. SEM Analysis

The CLA/PVA, CuO-CLA/PVA-1, and Cu-CLA/PVA-2 membranes prepared in this work all demonstrate good flexibility and are not easily fractured. Their surface morphologies were characterized by SEM. Fig. 13(a) shows that the CLA/PVA membrane veneer is smooth and contains granular carbon protrusions, indicating that the CLA and PVA exist in separate phases. On the reverse side of the membrane, massive agglomerates are visible, the surface flatness is significantly reduced, and a porous structure exists, indicating that carbon is deposited on the surface of the polymer PVA. Fig. 13(b) shows that the CuO-CLA/PVA-1 membrane veneer is also smooth and that the phase separation between the particles and the membrane is weaker than that of the CLA/PVA membrane. This indicates that the addition of nano-CuO significantly improves CLA dispersion. The particles on the reverse side of the CuO-CLA/PVA-1 membrane show a stacked morphology, and a

larger number of pore channels are formed by this stacking. The number of small particles entrapped in this membrane is significantly higher than that in CLA/PVA. Based on XRD and EDS analysis, these small particles are assumed to be the incorporated nano-CuO. Fig. 13(c) shows that the Cu-CLA/PVA-2 membrane veneer is less smooth than those of the other membranes. Rod-shaped particles are visible on the membrane surface, with some larger particles showing an irregular cubic configuration. The number of pores on the reverse side of the Cu-CLA/PVA-2 membrane is significantly lower than that of the other two membranes, indi-

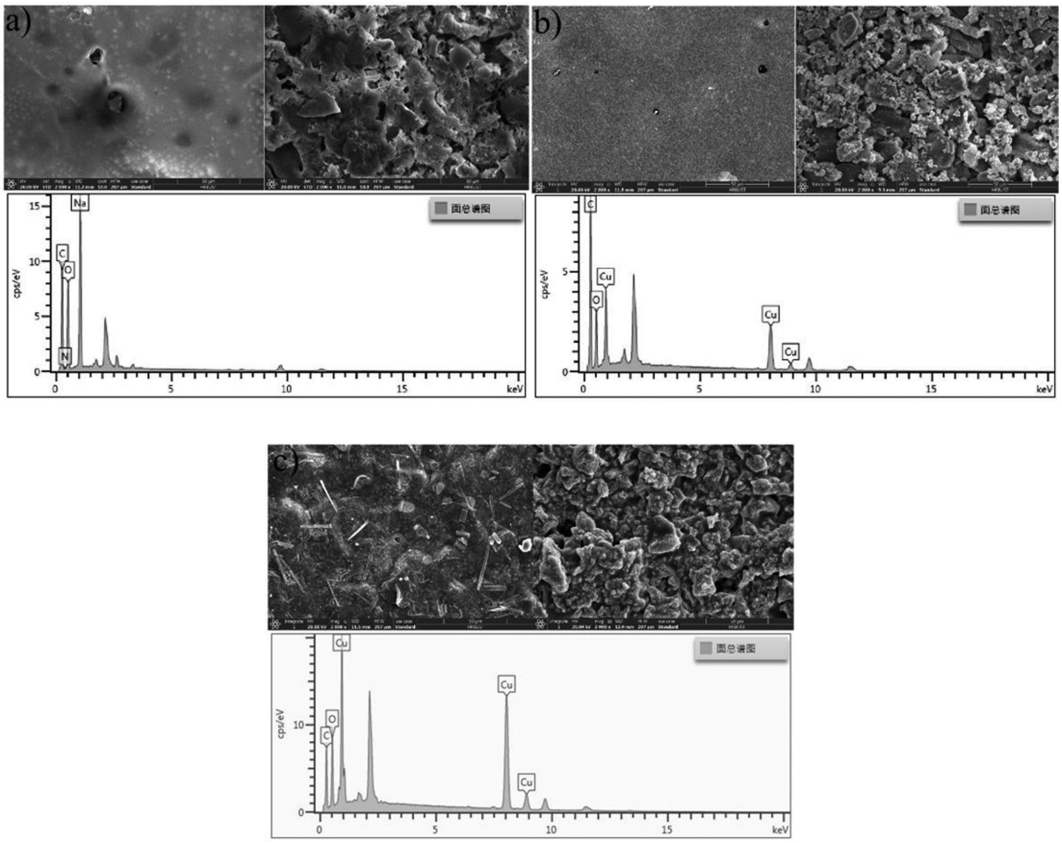

Fig. 13. SEM images of CLA/PVA, CuO-CLA/PVA-1, and Cu-CLA/PVA -2 membranes ((a) CLA/PVA; (b) CuO-CLA/PVA-1; (c) Cu-CLA/PVA-2).

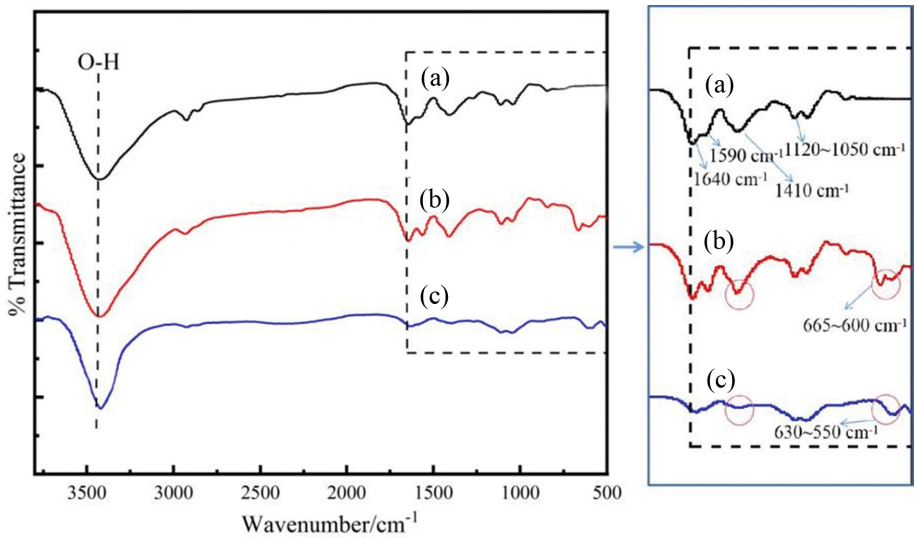

Fig. 14. FT-IR spectra of CLA/PVA, CuO-CLA/PVA-1, and Cu-CLA/PVA-2 membranes ((a) CLA/PVA; (b) CuO-CLA/PVA-1; (c) Cu-CLA/PVA-2).

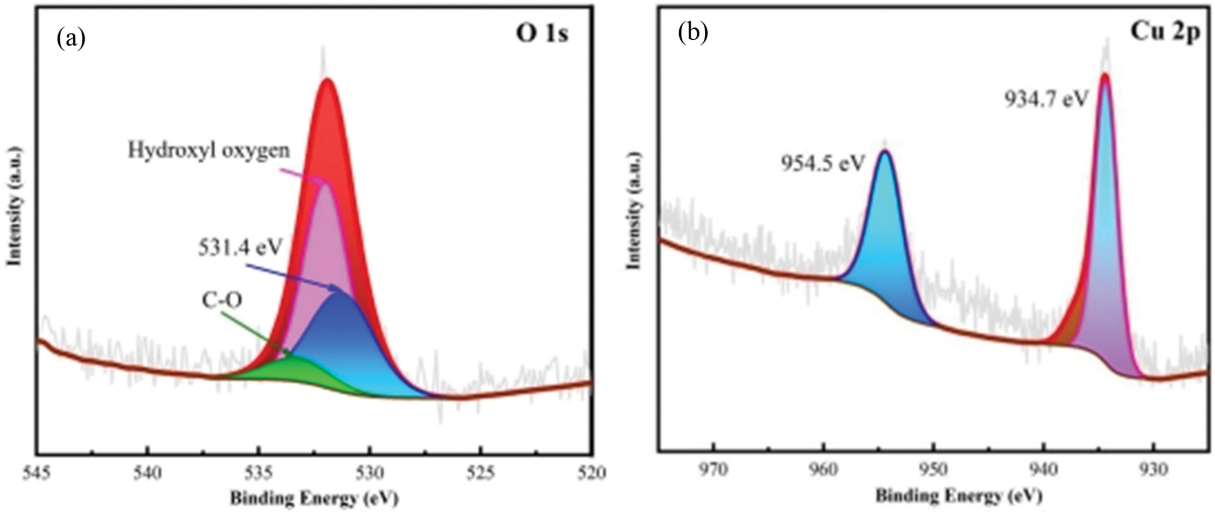

Fig. 15. High-resolution O 1s and Cu 2p XPS spectra of Cu-CLA/PVA-2 showing fitted peaks. (a) O 1s, (b) Cu 2p.

cating that the CuO formed by roasting is mainly distributed on the surface of CLA. This increases the CLA particle size and blocks some of the pore channels. The EDS results show that both the nano-copper blending method and the copper salt immersion method result in the successful doping of Cu into the membranes, and the copper content in Cu-CLA/PVA-2 is significantly higher than that in CuO-CLA/PVA-1.

2-3. FT-IR Analysis

Fig. 14 shows the FT-IR spectra of CLA/PVA, CuO-CLA/PVA-1, and Cu-CLA/PVA-2. As shown in Section 2.1, the deodorization performance of CLA/PVA is inferior to that of CuO-CLA/PVA-1 and Cu-CLA/PVA-2, demonstrating the weaker H_2S adsorption effect of porous materials without active components that solely rely on the physical adsorption effect of lignin carbon. In contrast, the Cu-containing membranes demonstrate superior H_2S adsorption performance due to the incorporation of the CuO active component. After preliminary analysis, it was concluded that some functional groups with adsorption activity might remain after alkali lignin charring at 400 °C, potentially enhancing adsorption. The FT-IR spectra absorbance bands of CLA/PVA, CuO-CLA/PVA-1, and Cu-CLA/PVA-2 are very similar, indicating that the addition of CuO does not affect the surface functional groups of CLA/PVA. A very strong broad absorption band at 3,000-3,300 cm^{-1} is ascribed to O-H stretching vibration. The spectral band at 1,050-1,120 cm^{-1} is attributed to the C-O-C stretching of acetyl groups present on the composite membrane backbone. The spectral band at 1,590-1,640 cm^{-1} corresponds to C=O stretching vibration. The spectral band at 1,410 cm^{-1} is caused by the C-H bending of $-CH_2$ in the composite membrane. Unlike the CLA/PVA spectrum, CuO-CLA/PVA-1 and Cu-CLA/PVA-2 exhibit stretching vibration peaks at 600-665 cm^{-1} and 550-630 cm^{-1}, respectively. These are the stretching vibration peaks of Cu-O. The 1,410 cm^{-1} peak of the CuO-CLA/PVA-1 spectrum is more intense than that of the CLA/PVA spectrum. This is mainly because the vibrations at this location partly originate from the surface atomic effect of the nano-CuO. The stretching vibrations of the vertical surface suspension bonds become extremely active in the presence of nano-CuO due to the greater proportion of surface atoms in the nanoscale powder. This leads to enhanced IR absorption intensity in this region [39]. The C=O stretching and $-CH_2$ bending vibration absorbance bands in the infrared spectrum of Cu-CLA/PVA-2 are significantly weaker than those of CLA/PVA and CuO-CLA/PVA-1. This indicates that loading CuO onto the lignin charcoal by impregnation leads to the CuO interacting with some of the hydroxyl groups in PVA, water, and propanetriol, weakening their peak intensity.

2-4. XPS Analysis

The chemical environment of the surface elements of the Cu-CLA/PVA-2 composite membrane was further analyzed by XPS. The O 1s and Cu 2p spectra fitting results are shown in Fig. 15. As shown in Fig. 15(a), the oxygen in Cu-CLA/PVA-2 exists in the form of C-O bonds, hydroxyl oxygen, and inorganic oxygen. The peak at 531.4 eV corresponds to the lattice oxygen binding energy of CuO. As shown in Fig. 15(b), the fitted peaks of Cu 2p are located at 934.7 eV and 954.5 eV. These peaks correspond to the Cu $2p_{3/2}$ and Cu $2p_{1/2}$ binding energies of the Cu 2p spectrum. This spectrum exhibits a narrow FWHM and no obvious vibration excitation peak, which is consistent with the previously discussed XRD results. Compared with the XPS signal standard CuO, the Cu 2p peak of the composite film is shifted toward a higher binding energy. This indicates that the chemical environment of the metal ions in the composite film is different than that of pure CuO. This is because the hydroxyl group of PVA is a negatively charged group with a higher electron binding energy [40]. The hydroxyl groups of PVA have electron lone pairs, which cause the electron density near copper atoms to increase. PVA therefore forms charge-transfer complexes through the coordination of its hydroxyl groups and copper.

CONCLUSION

In this paper, CLA/PVA composite membranes were prepared using a solution casting method and their H_2S adsorption performance was investigated. Based on the results reported herein, the following conclusions can be drawn:

1. The CLA/PVA membrane prepared using CLA demonstrates

better H_2S adsorption compared to CSL/PVA and SC/PVA. Using a water-to-alcohol ratio of 3 : 1 in the membrane precursor solution and 2 wt% CLA content leads to an optimal CLA/PVA membrane for H_2S adsorption. This membrane adsorbs H_2S for up to 30 min, and its mechanical strength and elongation at break values are 1.94 MPa and 120%, respectively.

2. The deodorization performance of copper-doped CLA/PVA is significantly improved compared to that of bare CLA/PVA. The Cu-CLA/PVA-2 membrane prepared by a Cu^{2+} doping impregnation method demonstrates better H_2S adsorption performance compared to the CuO-CLA/PVA-1 membrane prepared by nano-CuO co-doping. Increasing the copper content lengthens the H_2S adsorption time of these composite membranes. A Cu loading of 25 wt% in the Cu-CLA/PVA-2 membrane leads to a H_2S adsorption time of up to 75 min. Moreover, this membrane has an H_2S adsorption capacity of up to 0.27 mol/kg.

Structural analysis shows that the CLA is poorly ordered in the composite membranes and that all the copper is present as CuO. Furthermore, the functional groups on the surface of the composite membranes do not significantly change after copper doping. CuO-CLA/PVA-1 demonstrates good CuO and CLA particle dispersion within the membrane, a smooth membrane veneer, and significantly enhanced elongation at break and tensile strength values. In Cu-CLA/PVA-2, CuO is loaded on the surface of CLA, resulting in large particles. This membrane has higher tensile strength and a lower elongation at break compared to CLA/PVA.

The raw materials used to prepare the CuO-CLA/PVA-1 and Cu-CLA/PVA-2 membranes in this work are widely available and inexpensive. These two membranes have good mechanical properties and good H_2S adsorption performance. As adsorbents, these membranes can be used in petrochemical applications such as the production of low-sulfur oil and gas products, natural gas, and biogas. These membranes also show promise for the production of high-purity special gases, fuel cell feed gas, and in other ultra-deep desulfurization fields. Moreover, they are expected to have a very good treatment effect for organized and unorganized gas emissions.

DECLARATION OF COMPETING INTEREST

The authors declare that they have no known competing financial interests or personal relationships that could have appeared to influence the work reported in this paper.

DATA AVAILABILITY STATEMENT

Some or all data, models, or code that support the findings of this study are available from the corresponding author upon reasonable request.

Funding: This work was supported by the Guangdong Province Engineering Laboratory for Air Pollution Control Open-end Fund (20193236-09-05).

REFERENCES

1. Q. Yang, Y. Li, B. Cui, Z. Q. Yang, Z. B. Liu and Y. Z. Peng, *Acta Sci. Circumst.*, **39**(07), 2079 (2019).
2. L. Barelli, G. Bidini, L. Micoli, E. Sisani and M. Turco, *Energy*, **160**, 44 (2018).
3. X. Ma, B. K. Lin, X. Wei, J. Kniep and Y. S. Lin, *Ind. Eng. Chem. Res.*, **52**(11), 4297 (2013).
4. M. Mahdyarfar, T. Mohammadi and A. Mohajeri, *New Carbon Materials*, **28**(1), 39 (2013).
5. E. N. Lightfoot, T. W. Root and J. L. O'Dell, *Biotechnol. Prog.*, **24**(3), 599 (2008).
6. F. Wang, *Research on the controllable preparation and functional modification of gas separation carbon membranes*, MA thesis, Shenyang University of Technology, Shenyang (2020).
7. Y. H. Sim, H. Wang, F. Y. Li, M. L. Chua, T. S. Chung, M. Toriida and S. Tamai, *Carbon*, **53**, 101(2012).
8. N. Somsesta, V, Sricharoenchaikul and D. Aht-Ong, *Mater. Chem. Phys.*, **240**, 122221(2020).
9. Y. Liu, J. J. Xia, J. Y. Lin, Y. Zhang and S. T. Tong, *Chin. J. Environ. Eng.*, **10**(11), 6171 (2016).
10. X. C. Wang, F. F. Zhang and T. T. Jiang, *J. Funct. Mater.*, **45**(11), 11001 (2014).
11. M. S. Zeng, Y. Q. She, Y. B. Hu, L. J. Wu, M. J. Yuan, Y. Qi, H. Wang, X. L. Lin and Y. L. Qin, *Chem. Ind. Eng. Prog.*, **40**(08), 4573 (2021).
12. X. P. Yue, F. G. Chen and X. S. Zhou, *BioResources*, **6**(2), 2022 (2011).
13. S. Liu, W. Wei, S. Wu and F. Zhang, *J. Porous Mater.*, **27**(5), 1523 (2020).
14. T. Zhang and Q. Shen, *J. Cellul. Sci. Technol.*, **4**, 19 (2004).
15. L. Zhong, *Preparation and propertiesresearch of pore-size controllable carbonmembrane*, MA thesis, Donghua University, Shanghai (2006).
16. C. D. Tran, H. C. Ho, J. K. Keum, J. Chen, N. C. Gallego and A. K. Naskar, *Energy Technol.*, **5**(11), 1927 (2017).
17. Y. J. Li, F. Li, Y. Yang, B. C. Ge and F. Z. Meng, *J. Polym. Eng.*, **41**(4), 245 (2021).
18. J. Pang, *Preparation and capacitive performance of sodium lignosulfonate based porous carbons,* DE thesis, China University of Mining and Technology, Beijing (2018).
19. X. C. Wang, F. F. Zhang and T. T. Qiang, *J. Funct. Mater.*, **45**(11), 11001 (2014).
20. J. D. Zhua, C. Y. Yan, X. Zhang, C. Yang, M. J. Jiang and X. W. Zhang, *Prog. Energy Combust. Sci.*, **76**, 360 (2020).
21. K. B. Aadil and H. Jha, *Iran. Polym. J.*, **25**(8), 661 (2016).
22. I. Korbagv and S. Mohamed Saleh, *Int. J. Environ. Stud.*, **73**(2), 226 (2016).
23. C. Zhou, P. W. Li, Y. H. Qu, Z. M. Yang, Z. Y. He, C. Wang, Y. H. Liu, S. H. Song and L. J. Yu, *Chin. Polym. Bull.*, **2**, 9 (2021).
24. C. Y. Li, Q. Xin, H. Wu, R. Guo, Z. Tian, Y. Liu and Z. Jiang, *Energy Environ. Sci.*, **7**(4), 1489 (2014).
25. H. X. Wang, Y. Y. Wang, Z. Hu, Y. Bai and T. P. F. Xiao, *China Synth. Resin Plast.*, **37**(04), 28 (2020).
26. Y. Zhao and W. W. Ho, *Ind. Eng. Chem. Res.*, **52**(26), 8774 (2013).
27. C. P. Shi, X. H. Hao, F. Li, H. M. Li and M. Sun, *Packaging J.*, **3**(01), 62 (2011).
28. D. Montes, E. Tocuyo, E. González, D. Rodríguez, R. Solano, R. Atencio and A. Moronta, *Micropor. Mesopor. Mater.*, **168**, 111 (2013).
29. J. Koteswararao, S. V. Satyanarayana, G. M. Madhu and V. Venkatesham, *Heliyon*, **5**(6), e01851 (2019).

30. N. A. Al-Tayyar, A. M. Youssef and R. R. Al-Hindi, *Food Packaging and Shelf Life*, **25**, 100523 (2020).
31. X. Liu, X. Chen, J. Ren, M. Chang, B. He and C. Zhang, *Int. J. Biol. Macromol.*, **132**, 978 (2019).
32. A. Jayakumar, K. V. Heera, T. S. Sumi, M. Joseph, S. Mathew, G. Praveen and E. K. Radhakrishnan, *Int. J. Biol. Macromol.*, **136**, 395 (2019).
33. L. Bunmechimma, T. Leejarkpai and S. A. Riyajan, *Carbohydr. Polym.*, **240**, 116215 (2020).
34. Y. Gao, X. R. Shi, W. L. Liu, W. X. Wang, Y. F. Shen and J. Chen, *Acta. Mater. Compos. Sin.*, **33**(01), 53 (2016).
35. R. Sitthikhankaew, S. Predapitakkun, R. W. Kiattikomol, S. Pumhiran, S. Assabumrungrat and N. Laosiripojana, *EnergyProcedia*, **9**, 15 (2011).
36. Y. Li, L. J. Wang, H. L. Fan, J. Shangguan, H. Wang and J. Mi, *Energy Fuel*, **29**, 298 (2015).
37. F. Li, F. Meng, H. Wang, B. Ge, Y. Zhang and C. Yu, *New. J. Chem.*, **43**(44), 17494 (2019).
38. J. K. Rao, A. Raizada, D. Ganguly, M. M. Mankad, S. V. Satayanarayana and G. M. Madhu, *J. Mater. Sci.*, **50**(21), 7064 (2015).
39. W. L. Wang, D. S. Li, Z. J. Wang, H. L. Cui and G. L. Xue, *Chin. J. Inorg. Chem.*, **18**(8), 823 (2002).
40. T. Matsushima, Y. Kinoshita and H. Murata, *Appl. Phys. Lett.*, **91**(25), 253504 (2007).